Computational Materials Science 224 (2023) 112174

Contents lists available at ScienceDirect

Computational Materials Science

journal homepage: www.elsevier.com/locate/commatsci

Full Length Article

Comparison of adsorption capacity of water and hydroxide with collector reagents on geversite ($PtSb_2$) mineral surface: A DFT-D insights

Samuel S. Mangwejane, Peace P. Mkhonto *, Phuti E. Ngoepe

Materials Modelling Centre, University of Limpopo, Private Bag X1106, Sovenga 0727, South Africa

ARTICLE INFO

Keywords:
DFT-D
Geversite ($PtSb_2$) surfaces
Collectors
H_2O and OH
Adsorption energies, Electronic properties

ABSTRACT

The interactions of water, hydroxide and organic collectors with mineral surfaces are the key aspects that define the floatability behaviour of minerals. This study employed the density functional theory with dispersion correction (DFT-D) method to unravel the adsorption capacity and bonding behaviour of H_2O, OH^-, normal-butyl-xanthate (NBX^-), butyl-dithiocarbamate ($BDTC^-$), butyl-trithiocarbonate ($BTTC^-$) and dibutyl-dithiophosphate ($DBDTP^-$) with the $PtSb_2$ (100) surface. The adsorption energy of hydration was found less exothermic than that of hydroxylation, indicating that the OH^- had greater ability to interact with $PtSb_2$ surface compared to H_2O. The collector adsorption energies strength decreased in the order: BDTC > BTTC > NBX > DBDTP, and clearly the BDTC unveiled the superior exothermic adsorption. It was found that the collectors may easily displace water and OH^-, and attach on the mineral surface during flotation due to their strong binding than water and OH^-. However, since there was a greater probability of OH^- attaching on the surface, operating at low pH may be decisive in the flotation of $PtSb_2$ mineral. This study has compared the adsorption behaviour of various collectors with water and hydroxide and established the best conditions that may improve the flotation performance of $PtSb_2$ mineral.

1. Introduction

There is a general problem in the floatability of the arsenide platinum group minerals (PGMs) largely found in the Bushveld Complex such as sperrylite ($PtAs_2$) which possess a pyrite structure [1,2]. Based on the view that arsenic belongs to the same group as the antimony on the periodic table, it prompted the desire to investigate the $PtSb_2$ mineral named "geversite", which also has a pyrite structure [3] and has not been given much attention. The unravelling of the surface behaviour of $PtSb_2$ may also provide a platform to unlock the behaviour of the sperrylite. This also requires investigation of surface interactions with various collectors in order to improve their recoveries. Identifying a well performing collector reagent requires testing of different collectors on their adsorption strength. It is paramount that these be compared to the most crucial species that are present in the flotation pulp, such as water and sodium hydroxide (NaOH), which determine the wettability and pH, which may affect the attachment of collector on mineral surface, respectively. A previous study has shown that hydroxide bind stronger than water and xanthate on sperrylite ($PtAs_2$) [4]. However, there is no much knowledge on the bonding behaviour of H_2O, OH^- and collectors with platinum antimonide ($PtSb_2$) mineral. Therefore this study provides novelty in describing how water, hydroxide and collectors adsorb on the understudied $PtSb_2$ mineral surface that is lacking from both computational and experimental aspects. The $PtSb_2$ mineral has been reported to occur in association with sequential mineral ore deposit. The $PtSb_2$ mineral was firstly identified in Driekop mine of South Africa in the critical zone of the Bushveld Complex [3,5]. The dominance of geversite in the reefs is of vital worth for exploration and might unravel the recovery of the antimonides and arsenides minerals. The great abundance of the $PtSb_2$ minerals in various mines demands for a necessity to discover prospects to exploit its recovery by flotation process. In order to understand the surface behaviour and reactivity with collector of the geversite mineral, computational simulations can produce results that may give guide prior to experiments. There are fewer studies on $PtSb_2$ mineral; the previous work carried out was by Emtage [6], Damon et al. [7] and Ngoepe et al. [8]. Recently, we used density functional theory (DFT) to investigate oxidation, hydration, hydroxylation and xanthate adsorption on the geversite mineral surfaces [9]. However, the dispersion correction were not considered, which are crucial in describing and including the long-range interaction to the

* Corresponding author at: Materials Modelling Centre, University of Limpopo, Private Bag X1106, Sovenga 0727, South Africa.
E-mail address: peace.mkhonto@ul.ac.za (P.P. Mkhonto).

https://doi.org/10.1016/j.commatsci.2023.112174
Received 29 December 2022; Received in revised form 28 March 2023; Accepted 30 March 2023
Available online 8 April 2023

total energy for molecule/s adsorption on surfaces.

In the absence of extensive work reported on the $PtSb_2$ mineral study, the related structure of $PtAs_2$ was reviewed since it has been recently given much attention. Previous study of sperrylite using computational method reported that the ethyl xanthate (EX^-) binds stronger than diethyl-dithiocarbamate (DEDTC) and diisobutyl-dithiophospinate (DTPi). In addition it was also reported that hydroxide had stronger affinity than the collectors. This suggested that at elevated pH the collectors may experience a barrier of OH^- on the sperrylite surface [4]. In order to overcome the barrier of hydroxide on the surface, the flotation must be operated at low pH, where there is less favourable condition for hydroxide molecules attachment. Furthermore, there is still a need for novel collectors that have better affinity with high selectivity on the mineral surface and thus improves floatability. The selectivity is provided by organic molecules that have ability to bind stronger on mineral surfaces. Recently a study on design and synthesise of a novel s-triazine collector and its interaction with sulphide minerals using density functional theory (DFT) and microflotation was conducted and showed to perform better than xanthate and dithiocarbamate [10]. This suggested that there is a platform to design collectors to target the PGMs. Furthermore, it has been reported that for platinum metals, the organic reagents with O-, S-, and *N*-bearing components have functionalities and discriminatory to platinoids [11]. A previous study has investigated the replacement of DTC/DTP by trithiocarbonate (TTC) in the flotation of the Upper Group (2) (UG2) PGMs ore. It was found that TTC exhibited significant improvement in the rejection of gangue [12]. Previously, a DFT study showed that DTP binds stronger than ethyl xanthate and isobutyl xanthate on pentlandite surface [43]; however, it is not certain if the same behaviour will occur on geversite mineral surface.

The hydration of surfaces determines the wettability (i.e. hydrophobicity and hydrophilicity) of the minerals and significantly influences the oxidation route that defines the final oxidation product resulting in the obvious variation in the mineral oxidation process [4]. Recently a study indicated that sperrylite and platarsite oxidise preferentially though the As and S atoms on the surfaces [13]. Previously, the interactions of water with minerals surfaces have been conducted and indicated different modes of water orientations and binding energies on the surfaces. Ntoahae et al. reported a binding energy of −27.1 kJ.mol^{-1}, for water adsorption onto sperrylite which preferred the parallel geometry relaxation to the surface [14]. However, Waterson et al. reported that the raised ridged arsenic (As) atoms on sperrylite prevent a fully parallel geometry of water molecule, which resulted in flipped into hydrogen-down of water relaxation with adsorption energy of −29.0 kJ.mol^{-1} [4]. Recently, the water adsorption on $PtSb_2$ (1 0 0) surface, reported an adsorption energy of –32.19 kJ.mol^{-1} for full surface coverage [9]. Another study reported the preferential interaction of pentlandite ($Fe_4Ni_5S_8$) surface with water via surface Fe and the O atom [15].

In the current study a computational simulation method was used to investigate and unravel the adsorption capacity and bonding behaviour of various collectors (i.e. butyl-xanthate (BX^-), butyl-dithiocarbamate ($BDTC^-$), butyl-trithiocarbonate ($BTTC^-$) and dibutyl-dithiophosphate ($DBDTP^-$)) on the (1 0 0) surface of geversite. These collectors adsorption strength were compared to the full surface coverage adsorption energies of water and hydroxides. The adsorptions were performed using density functional theory adopting the dispersion correction (DFT-D) method. In addition the chemistry of bond formation are analysed from density of state (DOS) and atomic charges (Mulliken). The outcomes of this study are important for providing knowledge of enhancing the efficiency of PGMs minerals separation which may be applicable in the froth flotation process.

2. Materials and methodology

2.1. Computational method

The study employed the density functional theory with dispersion correction (DFT-D) for the bulk, surfaces and surface adsorptions. The Tkatchenko and Scheffler (TS) [16] dispersion method was adopted. In addition, the generalized gradient approximation with Perdew-Burke-Ernzerhof (GGA-PBE) exchange–correlation functional [17] was employed within the Cambridge Serial Total Energy Package (CASTEP) code [18]. The ultrasoft pseudopotentials were adopted in the study and the valence electron configurations considered for the atoms were: $5d^96s^1$, $5s^25p^3$, $3s^23p^4$, $2s^22p^4$, Ss^22p^2, Ss^22p^3, Ss^22p^3 and 1 s^1 for Pt, Sb, S, O, C, N, P and H, respectively. The plane wave cut-off energy of 500 eV which demonstrated convergence to within 0.2 meV.atom^{-1} and, k-points sampling of 8 × 8 × 8 and 4 × 4 × 1 as proposed by Monkhorst-Pack [19] were employed for bulk and surfaces, respectively. The convergence tolerance of force, ionic displacement and energy were 0.05 eV.Å^{-1}, 0.002 Å and 2.0 × 10^{-5} eV.atom^{-1}, respectively.

The geversite ($PtSb_2$) mineral possess space group symmetry of *Pa*-3 (2 0 5). Previously it was reported that for a system such as $PtAs_2$, inclusion of hydrostatic pressure widens the band gap of the material [20]. As such an inclusion of hydrostatic pressure was performed by varying pressures from 1.0 GPa to 5.0 GPa. However, it was found that the $PtSb_2$ does not produce any band gap from the band structures. This suggested that the $PtSb_2$ does not possess any band gap. However, it was noted that as the pressure increases, the lattice parameters reduced as shown in Fig. 1a. The relaxed bulk unit cell structure at 4.0 GPa as shown in Fig. 1b, possessed lattice vectors of $\alpha = \beta = \gamma = 90^\circ$ with cell size of a = 6.431 Å, this agreed well with the reported experimental findings of a = 6.428 Å [3], a = 6.440 Å [7] and calculated a = 6.441 Å [8].

The relaxed $PtSb_2$ bulk structure at 4.0 GPa was used to cleave the

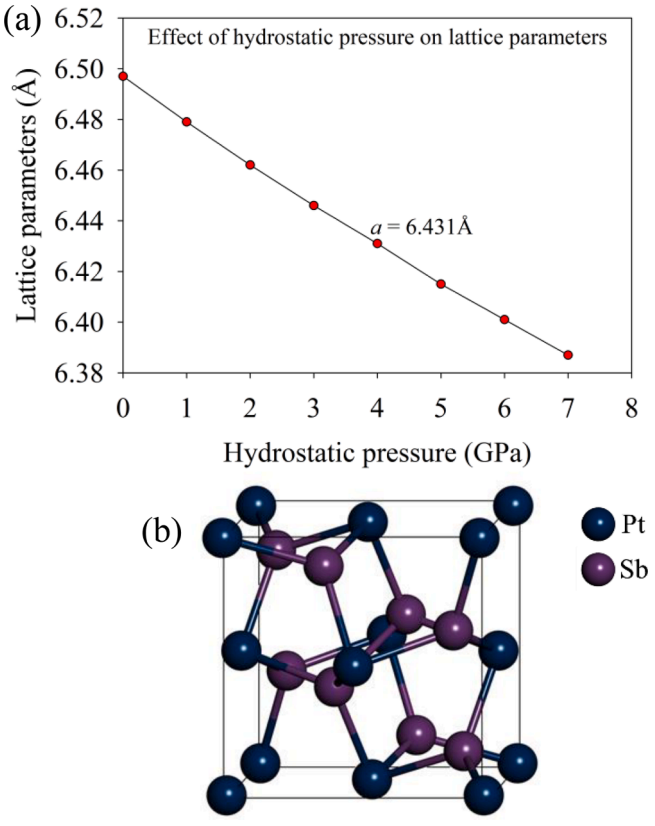

Fig. 1. (a) Effect of hydrostatic pressure on lattice parameters of bulk $PtSb_2$ and (b) relaxed bulk $PtSb_2$ model.

surfaces. Note that for surface studies, the pressure was not included. The adopted (1 0 0) surface slab had 12 layers and of 2 × 2 supercell, with a vacuum slab separation of 20 Å. This resulted in a periodic cell of 12.862 × 12.862 × 31.277 Å for (1 0 0) surface. During the adsorption systems, the bottom six layers (6L) were fixed, while the top six layers (6L) were allowed to relax. All adsorbate molecules were optimized at gamma point (1 × 1 × 1) and with other precision settings as in adsorption system. The H_2O and OH^- were relaxed in a 15 Å cubic box, while the collectors were relaxed in a 40 Å cubic box.

2.2. Energy calculations

The negative charge (-1) on OH^- and collectors were considered during their isolation optimization. The simplified Makov-Payne [21] was used to correct the total energies of the OH^- and collectors using equation (1) [4,21]:

$$E_{corr} = E_0 + (14.39952)\frac{q^2\alpha}{2L} \quad (1)$$

where the uncorrected total energy is denoted by E_0, adsorbate molecule charge by q, Madelung constant (2.8373 for cubic system) given by α [22] and unit cell vector length defined by L. These settings were also employed for the electronic properties calculation.

The zero-point energy (ΔZPE) was added to the computed adsorption energies in order to correct the computational simulations performed at 0 K. The ΔZPE was obtained from the difference between the ZPE of the surface-adsorbate system and ZPE of the isolated adsorbate gas phase, according to equation (2) [23,24]:

$$\Delta ZPE = \left(\sum_{i=1}^{3n}\frac{h\nu_i}{2}\right)_{S+NA} - \left(\sum_{i=1}^{3n}\frac{h\nu_i}{2}\right)_{Gas(A)} \quad (2)$$

where h = Planck constant, ν_i = vibrational frequencies in three dimensions and n = number of atoms in the adsorbate/s. Note that for the multi molecules adsorptions, the ZPE of one molecule in gas phase (i.e. $N = 1$) was multiplied by the number of molecules to give an equivalent ZPE to the number of adsorbates on the surface. The "One large supercell" was used to calculate the vibrational Phonons, where the supercell was defined by cut-off radius of 5.0 Å. A separation of 0.015 $Å^{-1}$ was adopted for the dispersion quality by selecting "Fine".

The adsorption energies ($E_{ads.}$) of uncharged (neutral) adsorbate (H_2O) to a surface were calculated from equation (3) [24]:

$$E_{ads.} = E_{[S+A]^0} - \left(E_{[S]^0} + NE_{[A]^0}\right) + \Delta ZPE \quad (3)$$

where $E_{[S+A]}$ = energy of adsorbed surface, $E_{[S]}$ = energy of clean surface, $E_{[A]}$ = energy of isolated adsorbate and N = number of adsorbates. Note that the superscript numbers denote either charged or neutral states. However, the collectors and hydroxide are negatively charged and therefore these adsorbates carry a formal negative charge. This suggested that the surface-adsorbate system should also carry a negative charge. This has been reported to presents a problem [4], and therefore the work function (WF = ϕ) was proposed by Neugebauer and Scheffler [25], to correct the extra electron in the electronic band structure. This was carried out by calculating the total energy of the $[S + A]^0$ system instead of $[S + A]^-$ system. The full details are shown in the Supporting Information (Section SI 1.2). Finally the adsorption energies for the charged OH^- and collectors adsorbates to a neutral surface were computed from equation (4) [24]:

$$E_{ads.} = \left(E_{[S+A]^0} - \phi_{[S+A]^0}\right) - \left(E_{[S]^0} + NE_{[A]^-}\right) + \Delta ZPE \quad (4)$$

A negative value in both equations (3) and (4) depict spontaneous exothermic reaction, whereas a positive value will divulge endothermic.

In this study, the surface energies ($E_{Surface}$) of the relaxed surfaces of the pristine symmetric and stoichiometric slabs were computed using equation (5) [26–29]:

$$E_{Surface} = \frac{E_{slab} - (n_{slab})(E_{bulk})}{2A} \quad (5)$$

where $E_{(slab)}$ = energy of the surface slab, $E_{(bulk)}$ = energy of the bulk per total number of atoms in the bulk and $n_{(slab)}$ = number of atoms in the surface slab model and A = surface area.

3. Results and discussion

3.1. Surface model, morphology and electronic structures

The $PtSb_2$ mineral surface cleaves perfectly along the (1 0 0) surface as the most stable surface similar to the pyrite [30] and sperrylite [4] minerals. In order to understand the mineral reactivity, it was paramount to investigate the chemical behaviour of the (1 0 0) surface prior to adsorptions. All possible terminations for low index (1 0 0), (1 1 0), (1 1 1) surfaces were explored as shown in the Supporting Information (Section SI 1.1). As explained by Tasker [31], the termination slab without perpendicular dipole moment were considered, i.e. Term (1 0 0)-B, Term (1 1 0)-B and Term (1 1 1)-C (see Fig. S1). All surfaces were constructed in (2 × 2) supercell having 96 atoms as shown in Table 1. The lowest relaxed surface energies of all slab surface termination are shown in Table 1, which were computed from equation (4). The $PtSb_2$ (1 0 0) surface exhibits lowest surface energy amongst the three surfaces and the surface stability decreases in the order: (1 0 0) > (1 1 1) > (1 1 0). These surface energies were lower than those reported by Ngoepe et al. [8] and the order of stability is different. However, the (1 0 0) surface energy is larger than our recently reported surface energy using DFT [9], as shown in Table 1.

The use of surface energies to calculate crystal morphologies provided good agreement with experiment as the difference in entropy between bulk and surface was small [32,33]. The Wulff [34] crystal morphology of geversite particle was constructed and produced under conditions of perfect thermodynamic equilibrium, vacuum and at 0 K from the surface energies in Table 1 as proposed by Gibbs method [35]. Recently, computational method was used to predict the morphology of cooperite [36], which produced irregular shape similar to those observed experimentally [37]. The calculated equilibrium morphology of geversite is expressed as a cubic shape with truncated corners and edges as shown in Fig. 2c, which was similar to sperrylite [13]. As expected, the (1 0 0) plane dominated the morphology, followed by the (1 1 1) surface that truncated the corners, while the (1 1 0) plane truncated the edges of the cube. The calculated ratios of the surfaces indicated that the (1 1 1) and (1 1 0) surfaces were expressed in the Wulff construction due to the surface energies ratio being less than $\sqrt{2} = 1.41$, that is $E_{Surf\text{-}(1\,1\,1)} / E_{Surf\text{-}(1\,0\,0)} = 1.09 < \sqrt{2}$, and $E_{Surf\text{-}(1\,1\,0)} / E_{Surf\text{-}(1\,0\,0)} = 1.29 < \sqrt{2}$. As such the (1 0 0) surface was the most preferred surface as shown on the Wulff equilibrium constructed morphology (Fig. 2c). In Fig. 2a and 2b, the unrelaxed and relaxed (1 0 0) surfaces are displayed. It was clear that the (1 0 0) surface was composed of Sb atoms on the 'Ridge' and Pt atoms in the 'Cleft', which is similar to sperrylite (1 0 0) surface model [38].

The density of states for the $PtSb_2$ bulk and (1 0 0) surface were

Table 1
Relaxed surface energies ($J.m^{-2}$) and atoms coordination of bulk and surfaces of $PtSb_2$ model.

Model	Number of atoms	Coordination		Surface energies	
		Pt	Sb	DFT-D	DFT [9]
Bulk	12	6	4	N/A	N/A
(1 0 0)-2 × 2	96	5	4	1.03	0.81
(1 1 0)-2 × 2	96	4	3, 4	1.32	1.08
(1 1 1)-2 × 2	96	5, 6	2, 3	1.12	1.07

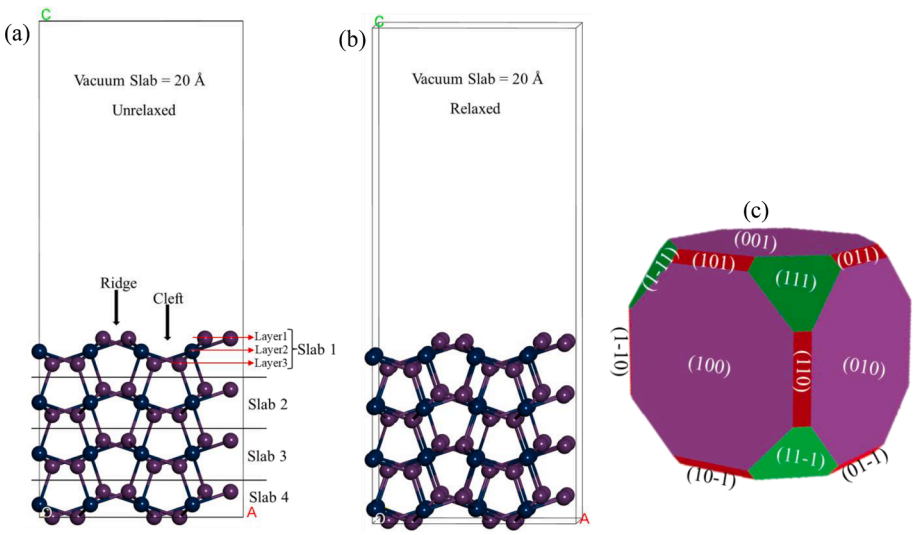

Fig. 2. The $PtSb_2$ (1 0 0) surface models: (a) unrelaxed surface, (b) relaxed surface, and (c) Wulff equilibrium surface morphology displaying the appearance of the (1 0 0), (1 1 0) and (1 1 1) surfaces.

computed and are shown in Fig. 3, which depict a metallic behaviour from the total density of states (TDOS). It was observed that the fermi energy (E_F) fell into the pseudo-gap for both bulk and surface density of states (DOS) suggesting stability. However, the pseudo-gap on the surface was not deep as compared to that on the bulk, thus the bulk had less states than the surface at E_F, which suggested bulk stability. Examinations of the PDOS it was found that the 5p-orbitals of Sb atoms contributed significantly at the E_F, while the 5d-orbitals and 6p-orbitals states of Pt atoms were almost at zero for both bulk and (1 0 0) surface (Fig. 3). Moreover, this showed that the Sb atoms are more active on the surface compared to the Pt atoms. The change of the pseudo-gap at the E_F on the surface compared to the bulk was due to the electrons depletion from valence band (VB) to conduction band (CB) predominantly occurring in the Sb 5s-orbitals and 5p-orbitals as shown in the partial density of states (PDOS). It was clear that the Sb atoms 5s-orbitals were raised at the CB, while the 5p-orbitals were lowered on the (1 0 0) surface, which indicated that surface cleavage resulted in change in coordination and therefore electron depletion (see Fig. 3b). The examination of the PDOS of the Pt atoms showed that the 5d-orbitals highest states split sharp peak on the bulk changed to almost smooth peak on the (1 0 0) surface. Importantly, it was noted that from the zoomed image at around 0.0 eV, the E_F cuts directly where the Pt 6p-orbitals and 5d-orbitals states intersect for the bulk PDOS (see Fig. 3a). However, on the (1 0 0) surface the Pt 6p-orbital had higher states than the 5d-orbitals at the E_F. This suggested that the 6p-orbitals contributed largely and therefore active orbitals on the Pt atoms. This indicated that there was electronic transition of electrons from the 6p-orbitals to the 5d-orbitals in the Pt atoms.

Table 2
Display the Mulliken atomic charges ($|e^-|$) for $PtSb_2$ bulk and (1 0 0) surface models.

Models	Atoms	s	p	d	Total	Charges
Bulk	Pt	6s = 1.00	6p = 1.32	5d = 9.00	11.32	−1.32
	Sb	5s = 1.45	5p = 2.90	5d = 0.00	4.34	+0.66
(1 0 0)	Pt	6s = 0.98	6p = 0.94	5d = 9.06	10.98	−0.98
	Sb	5s = 1.82	5p = 2.98	5d = 0.00	4.80	+0.20

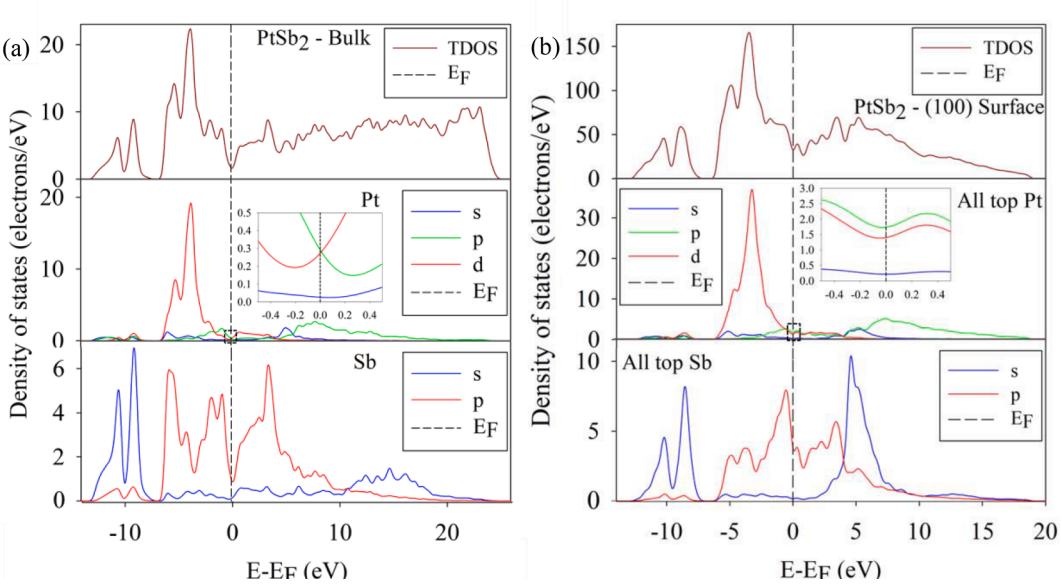

Fig. 3. The total and partial density of states (TDOS and PDOS) of $PtSb_2$ models: (a) bulk and (b) (1 0 0) surface model.

These effects are also depicted from the Mulliken atomic charges as displayed in Table 2, where the Pt atoms are less negative, while the Sb atoms are less positive at the (1 0 0) surface compared to the bulk. This indicated that surface cleaving results in loss of charges on the Pt atoms, while the Sb atoms gains charges, which was evident from the change at the E_F in the PDOS. This behaviour resulted in lone-pair of electrons on the Sb atoms at the 'Ridge', which was similar to the behaviour reported for $PtAs_2$ (1 0 0) surface by Waterson et al. [38]. Analysis of the orbitals charges revealed a slight change on the 6s-orbitals states of the Pt atoms, which suggested orbitals hybridisation between 6p-orbitals and 5d-orbitals of Pt atoms, and 5s-orbitals and 5p-orbitals of Sb atoms. A 0.37|e^-| charges gain was noted in the 5s-orbitals, with only 0.08|e^-| charges gained in the 5p-orbitals of Sb atoms on the surface. There was a greater charge loss on the 6p-orbitals (0.38|e^-|) which were almost equal to the charges gained on 5s-orbital of Sb, with only 0.06|e^-| charges gained in the 5d-orbitals of the Pt atoms on the surface (see Table 2). This showed that the mixing of the orbitals transferred electrons largely from the Pt 6p-orbitals to the Sb 5s-orbitals and 5p-orbitals during surface cleavage. This was also evident from the PDOS of Sb atoms, where the 5s-orbitals peaks were raised and shifted down in energy at the CB. Moreover, in this mixing, the 6p-orbitals also transferred charges to the 5d-orbitals within the Pt atoms.

3.2. Single and full monolayer surface coverage adsorption of water and hydroxide on $PtSb_2$ (1 0 0) surface

The water interaction with mineral surface depicts the hydrophobicity and hydrophilicity (i.e. wettability) in the wet-grinding and flotation process. On the other hand the hydroxylation of mineral surface depicts the pH effects in the flotation process, where the OH^- determine the interaction of NaOH with the mineral surface, after the sodium (Na^+) dissociate into solution. In order to understand the hydration and hydroxylation of surfaces, it requires a defined large number of water molecules to fill the vacuum slab for computation to accurately give these effects. However, for computational such as DFT this may require an extensive computing time requiring a large number of core, considering the degree of freedom of the water molecule to optimize and therefore large number of electrons in the system. In order to have a view of how water and hydroxide interacts with the surface, the single water and hydroxide molecule, and full monolayer surface coverage adsorption were explored. Note that the (2 × 2) supercell of $PtSb_2$ (1 0 0) surface is composed of exposed eight Pt sites and eight Sb sites available for adsorption; as such the full monolayer coverage consisted of 16 water/hydroxide molecules. The surface with number of molecules (*N*) is optimized separately and the water and hydroxide molecule/s adsorptions behaviour is examined in terms of adsorption energies (Table 3). The water and hydroxide molecule/s adsorptions were initially positioned on the (1 0 0) surface with the oxygen bonded to the Pt and Sb atoms at a distance of around 2.00 Å. The isolated water (H_2O) molecule relaxed to bond length of O_w—H = 0.977 Å and bond angle of H—O_w—H = 104.64°, while the isolated hydroxide (OH^-) molecule relaxed to bond length of O—H = 0.982 Å.

The results showed that, for single H_2O molecule adsorption on Pt and Sb atoms, the H_2O molecule adopts parallel and flipped-hydrogen-down to the surface, respectively. In both cases, it was found that water preferred to adsorb on the surface via the H atom and the H_2O molecule did not chemisorb on the surface, but adsorb through Van der Waals interaction (physisorption). A non-bonding distance of Pt1—O_w = 2.897 Å was noted. It was also noted that the water H atoms interacted with surface Sb for H_2O adsorption on Pt atom, where a Sb—H non-bonded distances of 2.832 Å and 3.211 Å were depicted (Fig. 4a). In the case of H_2O adsorption on Sb atom, the water molecule moved away leaving a non-bonded distance between Sb1—O_w of about 5.258 Å indicating a weak interaction due to flipped hydrogen down on the surface. Furthermore, a shorter Sb—H distance of 2.970 Å and 3.120 Å was depicted, suggesting strong interaction of the hydrogens with the Sb on the surface (Fig. 4b). The calculated adsorption energies of −1.12 kJ.mol^{-1} and −3.32 kJ.mol^{-1} were obtained for Pt and Sb adsorptions, respectively. This indicated a weak interaction of single water molecule with Sb and Pt atoms (Table 3).

The full monolayer coverage of H_2O molecules adsorption resulted in relaxation and position of water molecules parallel to the surface, while other H_2O molecules were positioned with flipped-hydrogen-down to the surface (see Fig. 5a). Concurrently, the O_w atoms interacted with H of the nearest H_2O molecule (H_2O—H-OH) as shown from the top view Fig. 5c, which also display the distances between the H_2O—H-OH in the packing geometries. Fig. 5c showed that the Pt and Sb atoms interacted with water molecules through H atoms, where only three Pt atoms interacted with water via O atoms (Pt—O_w) giving distances of 3.851 Å, 2.885 Å and 2.475 Å. The bond distance of 2.475 Å was similar to the reported Pt—O_w = 2.48 Å for H_2O adsorption on sperrylite surface [4]. The large Pt—O_w distances of 3.851 Å and 2.885 Å could be related to the reported distances (Pb—O_w = 2.950 Å, and 3.085 Å and 3.260 Å), found on hydrophobic galena surface, which was larger than the Fe—O_w = 2.253 Å found on hydrophilic pyrite surface [39], this suggested that geversite is hydrophobic. These findings indicated that water molecules adsorb on hydrophobic surface at above 3.0 Å distance of metal to oxygen distances. Due to dominant flipped-hydrogen-down water molecules, it was therefore evident that geversite mineral interacts with water mainly through H atoms.

The full monolayer coverage average adsorption energy was found as −42.66 kJ.mol^{-1}, which was larger than our previous reported binding energy of water on $PtSb_2$ (1 0 0) surface of −38.19 kJ.mol^{-1} using DFT [9]. The strong binding energy was attributed to the inclusive of dispersion correction in the current study which accounts for the long-range interactions of molecules on the surface, which were not included in the previous study. In addition, comparison to the reported adsorption energies of water on sperrylite of −27.1 kJ.mol^{-1} [14] and −29.0 kJ.mol^{-1} [4], the current adsorption energy was much stronger. This suggested that geversite (1 0 0) surface was more hydrophilic but had similar hydrophilicity to the sperrylite.

The bonding geometries of OH^- resulted in bent and the H atoms

Table 3
The adsorption energies of single and full monolayer coverage adsorption of H_2O and OH^- on $PtSb_2$ (1 0 0) surface, calculated according to equation (3) for H_2O and equation (4) for OH^-.

Adsorptions			Total energies (eV)			WF and ZPE (eV)		Adsorption energies (kJ.mol^{-1})	
Site	Adsorbate	*N*	$E_{[S+A]^0}$	*N* $E_{[A]^x}$	$E_{[S]^0}$	$\phi_{[S+A]^0}$	ΔZPE	$E_{ads.}$	$E_{ads.}$ /*N*
Pt	H_2O	1	−33183.975	−468.803	−32715.062	N/A	0.099	−1.12	−1.12
Sb	H_2O	1	−33183.989	−468.803	−32715.062	N/A	0.090	−3.32	−3.32
Pt	OH^-	1	−33167.013	−451.817	−32715.062	4.393	0.118	−425.42	−425.42
Sb	OH^-	1	−33167.887	−451.817	−32715.062	4.363	0.114	−507.23	−507.23
Full	H_2O	16	−40224.752	−7500.847	−32715.062	N/A	1.769	−682.60	−42.66
Full	OH^-	16	−39958.340	−7229.077	−32715.062	4.975	2.183	−1637.65	−102.35

Value of × is defined as: x = 0 for H_2O ($E_{[A]^0}$) and × = − 1 for OH^- ($E_{[A]^{-1}}$), and *N* = number of adsorbates.

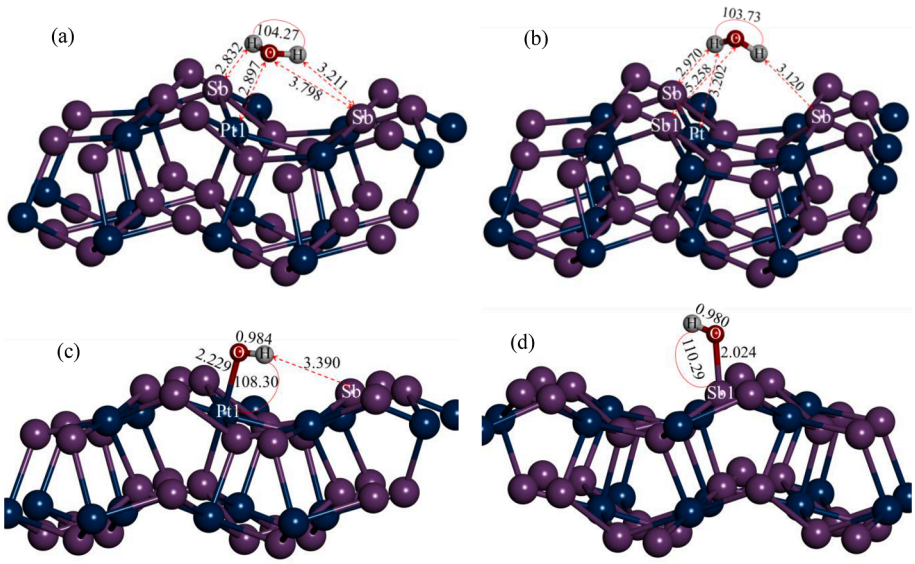

Fig. 4. Relaxed geometries for single adsorption of water and hydroxide on $PtSb_2$ (1 0 0) surface: (a) H_2O adsorption on Pt, (b) H_2O adsorption on Sb, (c) OH adsorption on Pt and (d) OH adsorption on Sb.

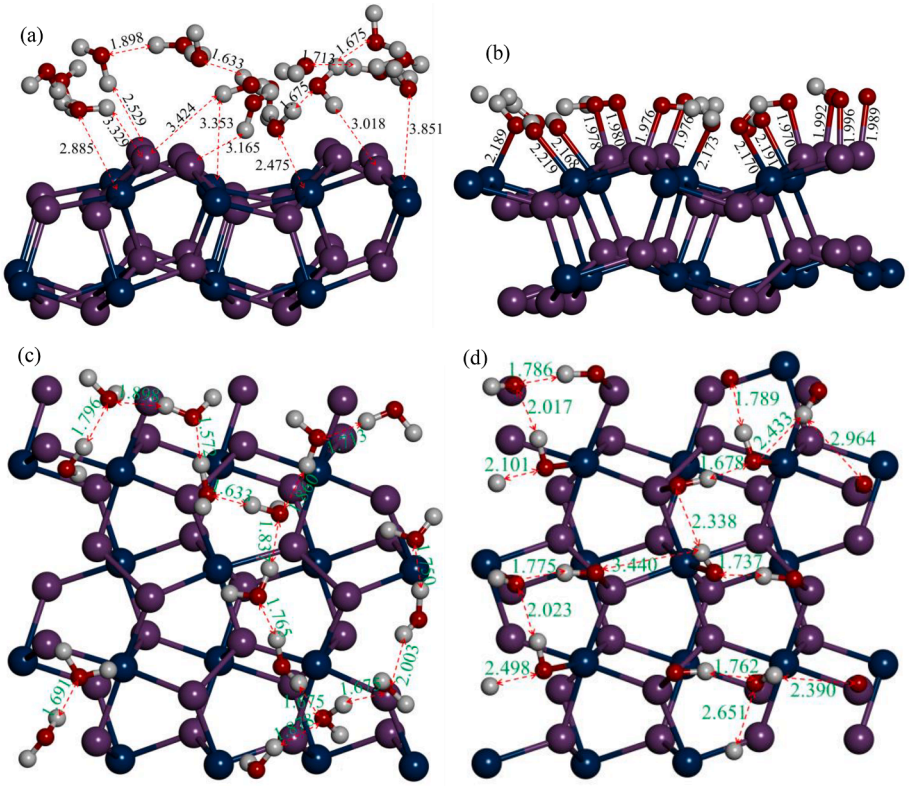

Fig. 5. Relaxed geometries for full monolayer surface coverage adsorption of water and hydroxide on $PtSb_2$ (1 0 0) surface: (a) side view of H_2O full monolayer, (b) side view of OH full monolayer, (c) top view of H_2O full monolayer and (d) top view of OH full monolayer adsorptions.

orientate parallel or at an angle to the surface. For single OH^- adsorption on Pt and Sb, this resulted in an angle of 108.30° and 110.29°, respectively (Fig. 4c and 4d). It was evident that the H atoms of OH^- had weaker interaction with the surface Pt and Sb atoms. The obtained adsorption energy for OH^- adsorption on Sb atom was −507.23 kJ.mol^{-1} which was more exothermic than for Pt atom adsorption with $E_{ads.} = -425.43$ kJ.mol^{-1} (Table 3). This was attributed to the Sb atoms being more active on the surface than the Pt atoms as depicted from the density of states of the clean (1 0 0) surface. In comparison with previous study of charged OH^- adsorption on Pt on sperrylite, where adsorption energy of −473.8 kJ.mol^{-1} was reported [4], there was some consistency with our findings for OH^- adsorption on Pt atom. A bond length of Sb–OH = 2.024 Å, which was shorter than that of Pt–OH = 2.229 Å was depicted, which correlated with the adsorption energies (see Fig. 4c and 4d).

The full monolayer coverage adsorption of OH^- on Pt and Sb atoms are presented in Fig. 5b and top view in Fig. 5d. It was clear that the OH^- remained bonded to the surface Pt and Sb atoms (see Fig. 5b). Looking at

Fig. 5d, the hydroxide oxygen atom interacted with the nearest H atoms of the OH^-, which also displayed the distances between the hydroxide O atoms and hydroxide H atoms (OH–-–OH) in the packing geometries. The average adsorption energy of −102.35 kJ.mol^{-1} was obtained for OH^- monolayer adsorption (Table 3). This current adsorption energy is less exothermic than our previous reported adsorption energy of −576.65 kJ.mol^{-1} for full monolayer coverage on $PtSb_2$ (1 0 0) surface using DFT [9]. From these results it was deduced that the OH^- had strong affinity with the $PtSb_2$ (1 0 0) surface through chemisorption than the H_2O molecules which were through physisorption.

3.3. Molecular geometry and electronic properties of collectors

The relaxed bond lengths for charged NBX^-, $BDTC^-$, $BTTC^-$ and $DBDTP^-$ models in their minimum energy geometries are shown in Fig. 6, with their relaxed bond distance shown in Table 4. Note that the main focus was on the two active sulphur atoms (i.e. S1 and S2) of the collectors. The sulphur atom (S1) possessed a double bond (C1=S1), while sulphur atom (S2) was single bonded and negatively charged (C1–S2$^-$). The C1–S bond lengths for BTTC were shorter amongst the collectors, which suggested that they were more stable, while those of BDTC were larger amongst the three collectors (NBX, BTTC and BDTC), suggesting that BDTC had high probability to be more reactive on the surface. The DBDTP possessed equal P—S bond lengths, which were larger compared to the C1–S bonds. It is shown in Table 4 that the bond angle (S1–C1/P–S2) of BTTC was larger, while that of DBDTP was smallest. Table 4 also display the selected torsion/dihedral bond angles of NBX, BDTC and BTTC molecules. Based on frontier molecular orbital (FMO) [40], it was suggested that the (O–C1(=S1)–S2$^-$) group lie almost in the same plane. This planar configuration favours formation of conjugated pie bonding (π–) or antibonding (π^*–). However, for DBDTP the torsion angles were around 129.14 and −129.14, which suggested difficulty in formation of conjugated π– or π^*–bond.

In this study, it was proposed that the adsorption strength of thiol collectors can be derived from the electron density of the S atoms, which are the centre of reactivity. As such the greater the negative charge on S atoms the stronger adsorption power. It was found that the S atoms of DBDTP possessed greater negative charges as depicted from Table 5, and the order of adsorption power therefore decreased in the order: DBDTP > BDTC > NBX > BTTC. However, the DBDTP may withhold its electron density due to the positively charged phosphorus atom, thus it may be weaker amongst the collectors and the adsorption power was therefore based on the order of BDTC > NBX > BTTC. Furthermore, the reactivity of these collectors was determined based on the calculated band structures band gaps. It was reported that a molecule with the lowest H-L gap or small band gap has the highest probability to have strong reactivity than the molecule with a larger gap [40]. It is shown in Table 5 that the BDTC had the smallest band gap, therefore it was proposes to possess a stronger reactive character and the reactivity order decreased as: BDTC > NBX > BTTC > DBDTP. These clearly suggested that the DBDTP may have weaker affinity with the surface amongst the collectors, while the BDTC exhibit stronger affinity.

Table 4
Display the relaxed bond lengths (R, in Å), bond angles (θ, in deg.°) and torsion/dihedral angle (Φ, in deg.°) for NBX^-, $BDTC^-$, $BTTC^-$ and $DBDTP^-$ isolated collectors.

Bonds	NBX^-	$BDTC^-$	$BTTC^-$	$BDTP^-$
R(C1/P=S1)	1.691	1.703	1.682	1.970
R(C1/P–S2$^-$)	1.683	1.710	1.686	1.972
R(C1/P—O/N/S3)	1.402	1.381	1.791	1.630
θ(S1=C1–S2)	128.31	126.93	129.15	119.22
Φ(S1=C1–S2–O/N/S3)	179.81	179.85	179.62	129.14
Φ(S2–C1= S1–O/N/S3)	−179.79	−179.85	−179.58	−129.14

Table 5
The calculated band gaps (eV) and atomic population (Mulliken) charges (|e$^-$|) for NBX^-, $BDTC^-$, $BTTC^-$ and $DBDTP^-$ isolated collectors.

Collector	Band gap	S1	S2	C1/P	O/S3/N
NBX^-	1.268	−0.36	−0.33	−0.11	−0.43
$BDTC^-$	1.159	−0.41	−0.43	−0.16	+0.55
$BTTC^-$	1.623	−0.30	−0.30	−0.46	+0.15
$DBDTP^-$	1.831	−0.75	−0.75	+1.48	−0.73

In Figs. 7 and 8 the total density of states (TDOS) and partials density of states (PDOS) for the collectors head group (i.e. –O/S3/N–C1/PS_2) are displayed, which are the polar group and possess the greatest influence in the reactivity of the collector on the mineral surface. The PDOS clearly showed that the fermi energy (E_F) cuts the sulphur 3p-orbitals peak, which suggested that they were not fully occupied, similar behaviour have been reported [29,41]. It was noted that the band gap on the S atoms is located at the conduction band (CB) just above the E_F, suggesting indirect band gap. From the PDOS, it was evident that the 3p-orbitals of S atoms contributed significantly at the E_F, thus the centre of reactivity. The S 3p-orbitals for NBX, BDTC and DBDTP are characterised by a broad peak which split into two peaks at its highest point (see Fig. 7a, 7b and 8b). The BTTC displayed a 3p-orbital broad sharp peak, which was cut by the E_F (Fig. 8a). The sharp peak at the CB on C1 and P shows that the LUMO or ability to accept electrons are largely localised on these atoms. Interestingly, the LUMO peaks on C1 and P atoms were of s,p-orbitals hybridisation character. Furthermore, the O and C1 of NBX, BDTC and BTTC possess a band gap at the E_F, which demonstrated that they were less reactive. Moreover, C1 and S1 atoms are characterised by an s,p-orbital hybridisation at around 6.5 eV which suggests an overlap of orbitals at this energy for these atoms as displayed on Figs. 7 and 8a. These findings suggested that the collectors S atoms

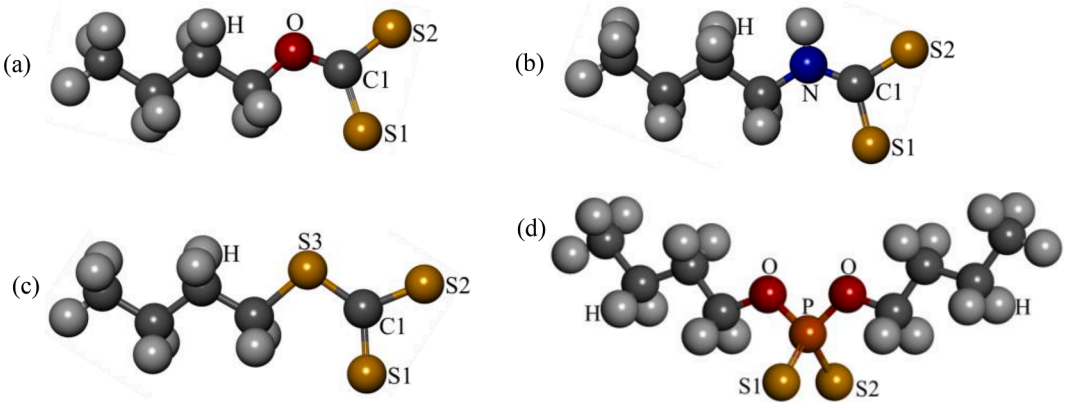

Fig. 6. Relaxed geometries of isolated collectors: (a) NBX^-, (b) $BDTC^-$, (c) $BTTC^-$ and (d) $DBDTP^-$.

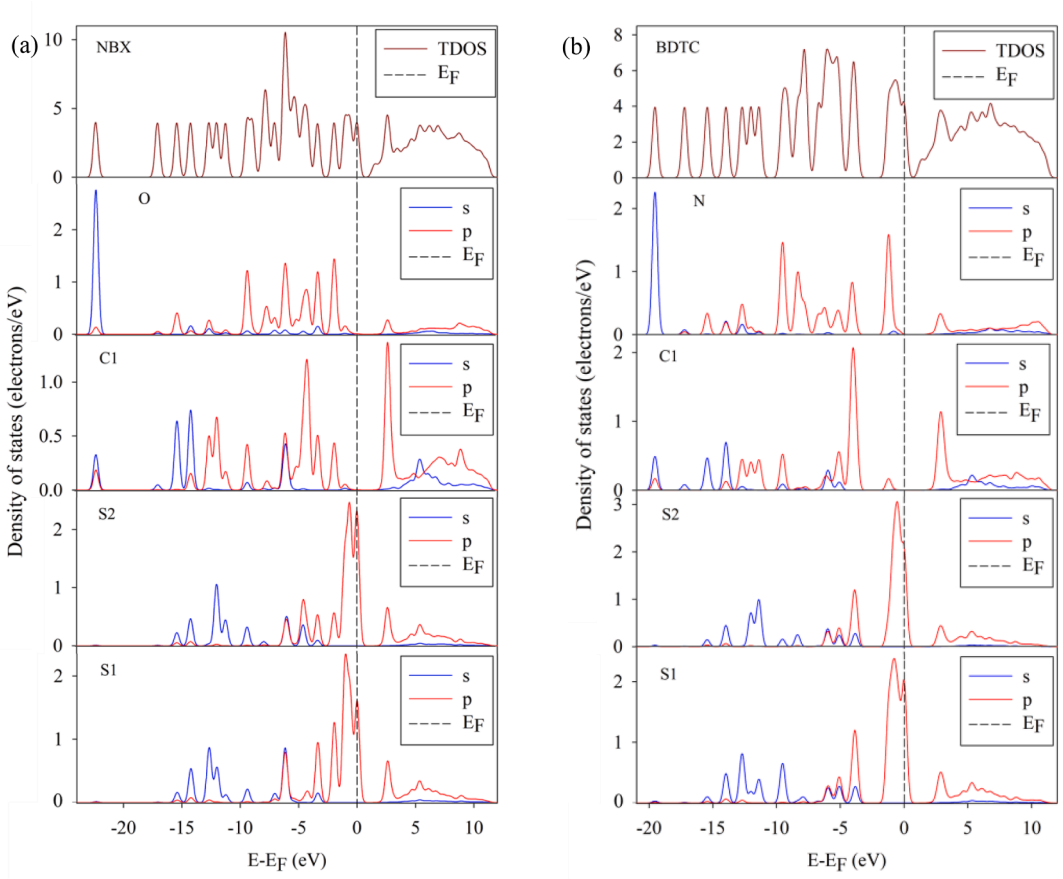

Fig. 7. The density of states (TDOS and PDOS) for the isolated collectors: (a) NBX^- and (b) $BDTC^-$ collectors.

have ability to form covalent bonds on surface of $PtSb_2$ mineral by offering their HOMO electrons to Pt atoms and concurrently the Sb atoms offer electrons from the 5p-orbital to the LUMO of the collectors S atoms.

3.4. *Adsorption of NBX^-, $BDTC^-$, $BTTC^-$ And $DBDTP^-$ Collectors onto $PtSb_2$ (1 0 0) surface.*

In the microcalorimetry experiment tests, the collector reagents are titrated on the mineral surfaces to measure the heats of adsorption and therefore affinity of collector with the mineral surface. Usually this gives the highest heats of adsorption at first collector addition and reduces as more collector molecules are added signifying saturation of the mineral surface. The highest heat of adsorption shows that the collector molecule binds on the most exothermic preferred site on the mineral surface [42]. This also predicts the performance of collectors during flotation. Similar behaviour can be extrapolated from computational calculation by testing different adsorption sites in order to predict and describe the most desired site for collector molecule on the surface. In this study, ten models for the collector adsorption on geversite (1 0 0) surface were obtained; all in their relaxed geometries as shown in the Supporting Information (Section SI 1.3). The relaxed most stable exothermic models are shown in Fig. 9. Out of the ten adsorption modes, six bridging-bidentate adsorptions of collectors were performed: [Pt1–S1, Pt2–S2]; [Sb1–S1, Pt1–S2 (F)]; [Sb1–S2, Pt1–S1 (F)]; [Sb1–S1, Pt1–S2 (N)]; [Sb1–S2, Pt1–S1 (N)] and [Sb1–S1, Sb2–S2]. Note that the Sb1–S1, Pt1–S2 (F) bridging was between Pt and Sb atoms that are far from each other, while the Sb1–S1, Pt1–S2 (N) bridging was between Pt and Sb atoms that are near and bonded to each other (see Fig. S7). Furthermore, two monodentate were explored, where only the negatively charged S2 atom of the collector anion attached to a surface Pt or Sb atoms (Sb1–S2 or Pt1–S2). In addition, the chelating-monodentate, in which both collector S atoms were attached on the same Pt or Sb atom on the surface, were investigated (S1–Sb1–S2 and S1–Pt1–S2). The adsorptions of the collectors were initially positioned at a distance of around 2.00 Å on Pt and Sb atoms.

Table 6 shows the computed adsorption energies for the most exothermic adsorption for each collector, while the adsorption energies of less exothermic adsorption sites are given in the Supporting Information (Table S2, S3, S4 and S5 of Section SI 1.3). It is shown in Fig. 9 that the bridging-bidentate on Pt and Sb was more exothermic and thus the most preferred site for the collectors' adsorption. The NBX was found to give preferred stable exothermic adsorption when positioned on Sb1–S1, Pt1–S2 (F) bridging-bidentate (see Fig. 9a). The BDTC was more exothermic when initially adsorbed on Sb1–S2 monodentate, which resulted in bridging-bidentate on Pt and Sb atoms (see Fig. 9b). The BTTC and DBDTP collectors also gave an exothermic stable adsorption when initially attached on Pt1–S2 monodentate, which also resulted in bridging-bidentate on Pt and Sb atoms as shown in Fig. 9c and 9d, respectively. Interestingly, only the DBDTP collector relaxed to Sb1–S1, Pt1–S2 (N) bridging-bidentate, while the NBX, BDTC and BTTC collector relaxed to Sb1–S1, Pt1–S2 (F) bridging-bidentate. It was observed that although the NBX, BDTC and BTTC collectors were initially positioned vertical on the surface, they relaxed to a flat position on the surface. This indicated that they prefer a flat adsorption mode and showed strong interaction of the hydrocarbon chain with the surface. Similar preferential flat adsorption of collectors has been recently reported on pyrite surface [10]. Therefore, for all collectors' adsorptions the dispersion long-range interaction of the hydrocarbon chain with surface largely contributed significantly to the adsorption energies.

Table 7 shows the bond lengths and angles for the collectors adsorptions on the $PtSb_2$ (1 0 0) surface. It was noted that for all collectors adsorption the S1 atom interacting with Sb1 atom (Sb1–S1) formed a

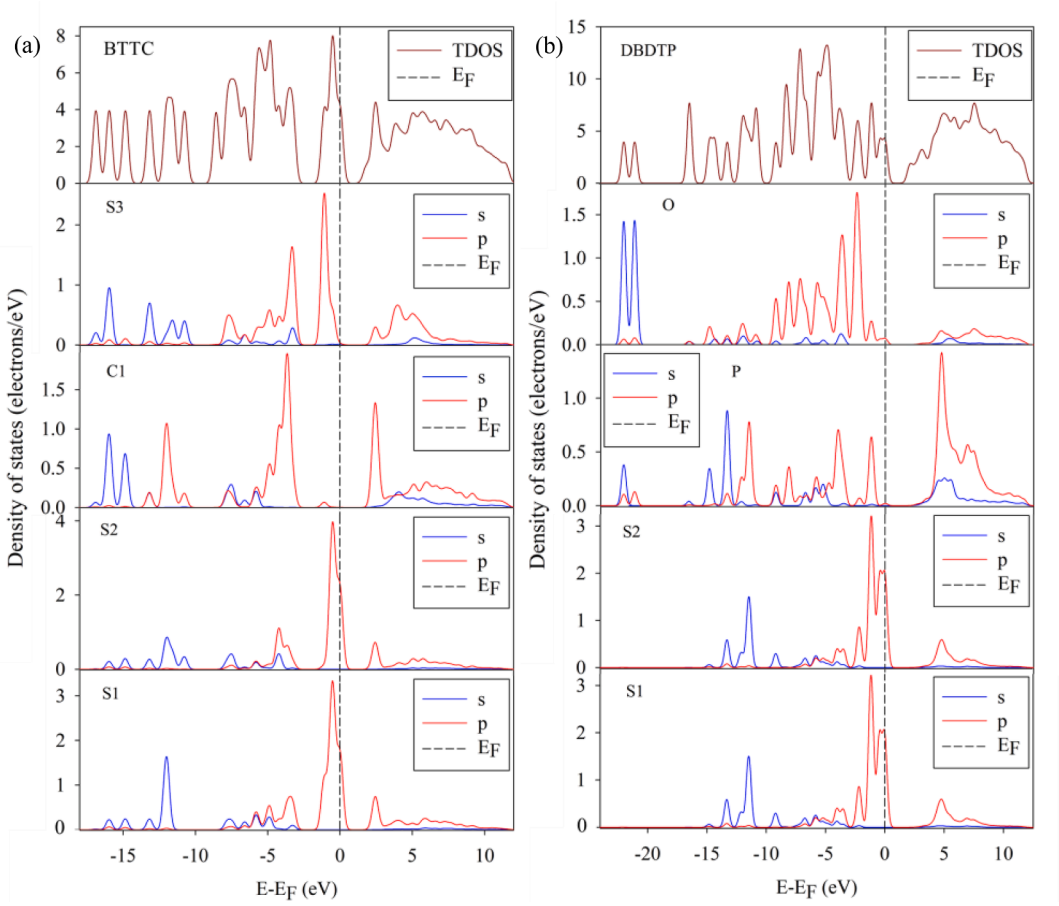

Fig. 8. The density of states (TDOS and PDOS) for the isolated collectors: (a) $BTTC^-$ and (b) $DBDTP^-$ collectors.

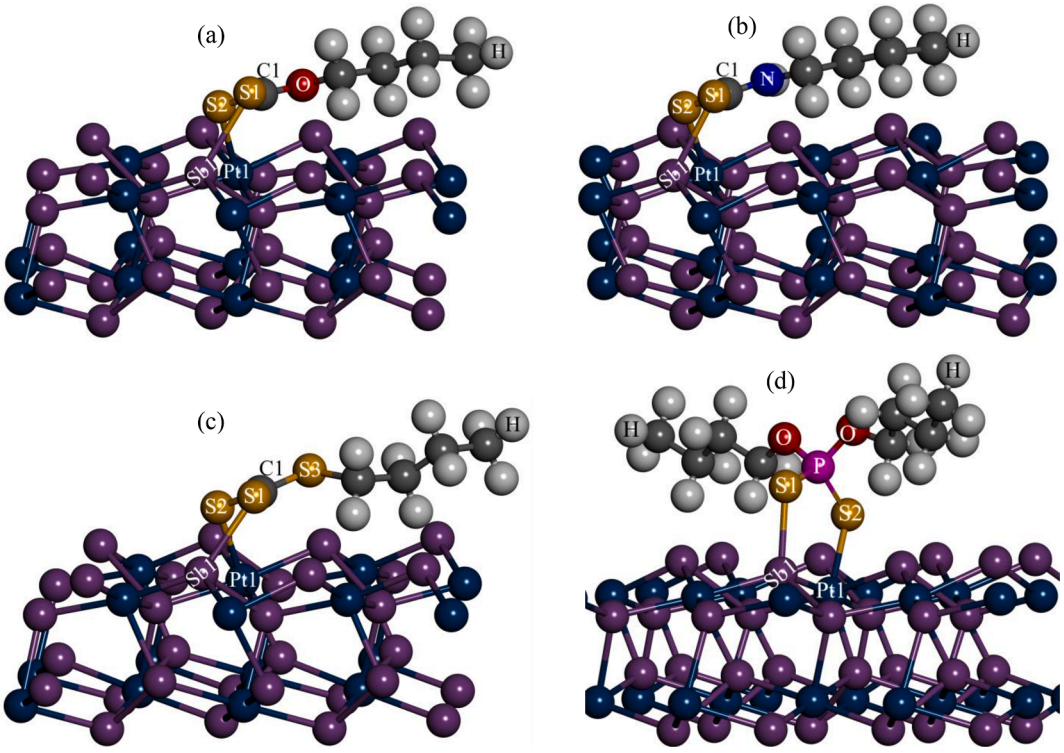

Fig. 9. Relaxed geometries for collectors adsorption on $PtSb_2$ (1 0 0) surface: (a) NBX^-, (b) $BDTC^-$, (c) $BTTC^-$ and (d) $DBDTP^-$ adsorptions.

Table 6
The adsorption energies of NBX^-, $BDTC^-$, $BTTC^-$ and $DBDTP^-$ collectors adsorption on $PtSb_2$ (1 0 0) Surface, calculated according to equation (4).

Collector	Binding Mode	$E_{[S+A]^0}$ (eV)	$E_{[A]^-_{Corr}}$ (eV)	$E_{[S]^0}$ (eV)	$\phi_{[S+A]^0}$ (eV)	ΔZPE (eV)	$E_{ads.}$ (kJ.mol^{-1})
NBX^-	Bridging-bidentate	−34628.010	−1913.526	−32715.062	4.224	−0.177	−368.82
$BDTC^-$	Bridging-bidentate	−34479.642	−1764.635	−32715.062	4.184	−0.082	−406.38
$BTTC^-$	Bridging-bidentate	−34469.811	−1755.295	−32715.062	4.264	−0.131	−371.49
$DBDTP^-$	Bridging-bidentate	−35857.495	−3143.214	−32715.062	4.137	−0.464	−362.51

Table 7
The relaxed bond length (*R*, in Å) and bond angles (θ, in deg.°) for NBX^-, $BDTC^-$, $BTTC^-$ and $DBDTP^-$ collectors adsorption on $PtSb_2$ (1 0 0) surface.

	Bond lengths and angles			
Bonds	NBX^-	$BDTC^-$	$BTTC^-$	$DBDTP^-$
R(Pt1–S2)	2.496	2.519	2.524	2.510
R(Sb1–S1)	2.772	2.634	2.688	2.584
R(C1/P–S1)	1.700	1.724	1.708	2.049
R(C1/P–S2)	1.715	1.731	1.711	2.011
θ(S1–C1/P–S2)	119.34	119.44	119.72	117.77

larger bond length than the S2 atom interacting with Pt1 atom (Pt1–S2). The C1/P—S bonds increased compared to the isolated collector models, suggesting weaker bonds. The bond angles (S1–C1/P–S2) of the NBX, BDTC and BTTC collector after adsorption reduced from 128.31°, 126.93° and 129.15° (isolated collectors) to 119.34°, 119.44° and 119.72° (after adsorption), which was owed to the bridging mode and flat orientation on the surface. However, the DBDTP changed from 119.22° (isolated collectors) to 117.77° (after adsorption).

The obtained most exothermic adsorption energies follow the order: BDTC > BTTC > NBX > DBDTP as shown Table 6 and depicted in Fig. 10. This showed that the N-bearing BDTC collector was more exothermic amongst the collectors. This indicated that BDTC was more reactive and had greater ability to donate electrons to the mineral surface. It was clear that the BTTC had strong binding to the surface compared to DBDTP and therefore may replace the DBDTP in the floatation of PGMs as previously reported [12]. Although the band gaps predicted the reactivity order as (i.e. BDTC > NBX > BTTC > DBDTP), there was a flip between NBX and BTTC, where the BTTC gave slight stronger adsorption than NBX. This suggested that the S-bearing collector (BTTC) had strong adsorption than the O-bearing collector (NBX). This was attributed to the S-linking atom being an electron donor, while the O-linking atom was an electron acceptor. However, it is proposed that in the presence of water the adsorption order may be different. The current adsorption energy of NBX (−368.82 kJ.mol^{-1}) was found more exothermic than our previously reported adsorption energy of −324.52 kJ.mol^{-1} for nBX adsorption on $PtSb_2$ (1 0 0) surface using DFT [9],

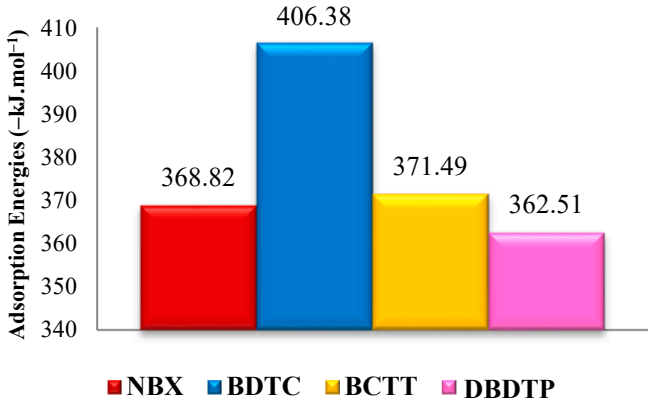

Fig. 10. Display the bar graph for the most exothermic adsorption energies trend for collectors adsorption on $PtSb_2$ (1 0 0) surface.

which is ascribed to inclusion of dispersion correction.

In comparing the adsorption energies of the full monolayer coverages of H_2O to that of OH^-, the results showed that hydroxide had stronger adsorption than water by more than half, which suggested a strong interaction of hydroxide on the mineral surface. In addition, this suggested a strong probability of hydroxylation of the surface at elevated pH. This behaviour articulate a probable barrier for adsorption of collector on mineral surface to render hydrophobicity during flotation, thus a strong collector would be required to displace these OH^- molecules. Alternatively, adjusting the pulp to lower pH would be beneficial to reduce the probability of surface hydroxylation. However, the comparison of the adsorption energies of the collectors to those of full monolayer coverages of H_2O and OH^-, it was found that the collectors had stronger adsorption, which suggested a strong interaction and ability of the collectors to overcome the barrier of the water and hydroxide on the mineral surface during flotation. As such the competition between hydroxylation and collectors can be overcome by adjusting the pH to acidic or neutral to favour the collector attachment on the surface during flotation. The optimal favourable pH condition requires experimental tests, thus this work only predict the possible condition and reduces the extensive flotation tests.

3.5. *Electronic properties of collectors and $PtSb_2$ (1 0 0) surface adsorptions.*

The PDOS and Mulliken atomic charges for the adsorptions of NBX^-, $BDTC^-$, $BTTC^-$ and $DBDTP^-$ collectors on the (1 0 0) surface are presented and analysed. Fig. 11 shows the PDOS of the surface Pt and Sb atoms before and after adsorption with collectors and in Fig. 12 and Fig. 13, the PDOS of before and after adsorption of the collectors' S atoms are presented. These properties gave detailed insights in the collector anions adsorption electronic behaviour on the surface and therefore their chemistry of adsorption. In Fig. 11a the Pt atoms 5d-orbital broad peak changed at the valence band (VB), where it split largely after interacting with DBDTP, while after interacting with NBX, BTTC and BDTC the peak split was minimal and almost the same as before adsorption. Interestingly, at the E_F, the Pt 6p-orbitals were lowered in states and the behaviour was similar to that of the bulk Pt atoms, which was due to formation of the six-membered group. However, due to the S atoms being less electron donor compared to the Sb atoms, the states could not behave exactly as the bulk model. Examination of the Sb atoms as shown in Fig. 11b, a clear reduction in the 5p-orbitals p1 peak states was noted at the VB. Furthermore, it was observed that the p2 peak increased in states at the CB for DBDTP collector adsorption; while for the other collectors there were slightly changed. It was observed that the p3 peak slightly increased in states for NBX, BTTC and BDTC and increased more for DBDTP (see Fig. 11b). These observations indicated that the Sb atoms lost electrons to the collectors S atoms. Interestingly, the E_F moved towards the pseudo-gap at the CB suggesting stability of the adsorptions. The collectors PDOS changes were examined as shown in Figs. 12 and 13. A clear shift of the 3p-orbitals peaks to the VB was observed and the E_F fell into the pseudo-gap, suggesting a stable adsorption. In addition, the 3p-orbitals peaks at the E_F reduced states, and concurrently shifted down in energy towards the VB. This indicated stability bonding, and since their states were reduced, it was suggested that they lost electrons.

The analysis of the electron gain and loss was depicted from the atomic charges displayed in Table 8. It was shown that both Sb and

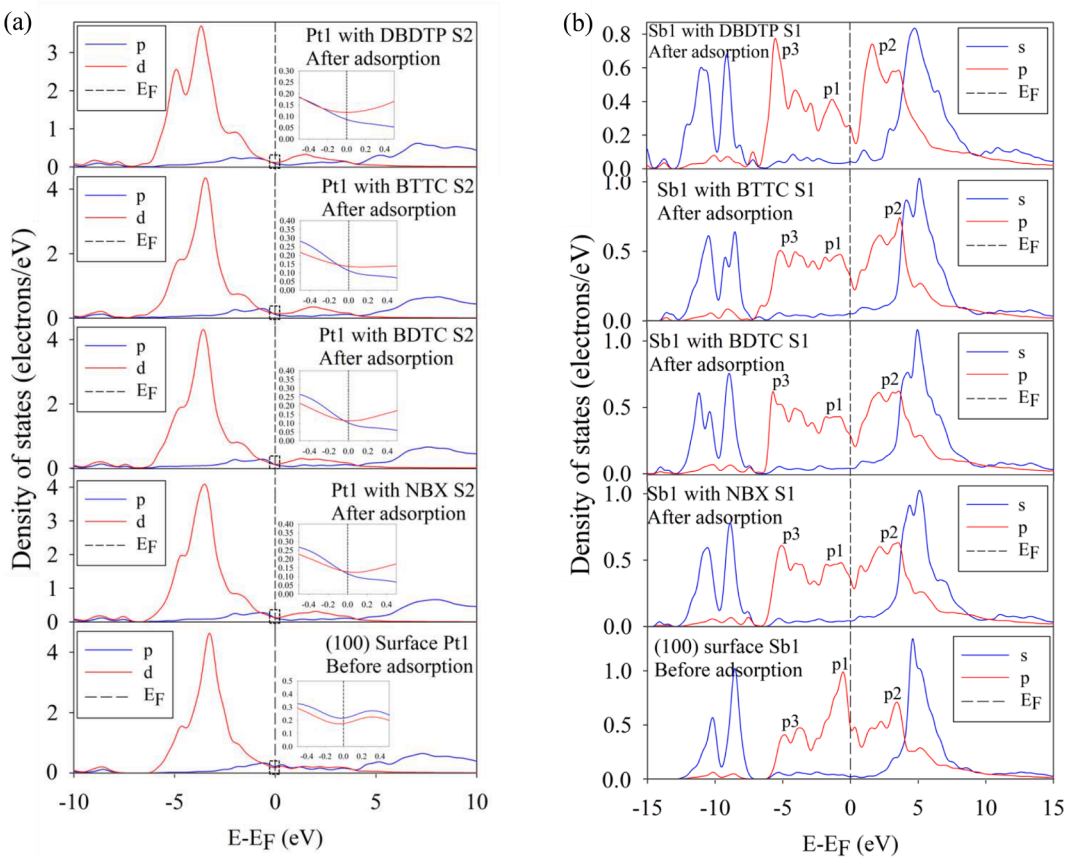

Fig. 11. The partial density of states (PDOS) of surface Pt and Sb atoms before and after adsorption with NBX^-, $BDTC^-$, $BTTC^-$ and $DBDTP^-$ collectors on $PtSb_2$ (1 0 0) surface: (a) Pt atoms PDOS and (b) Sb atoms PDOS.

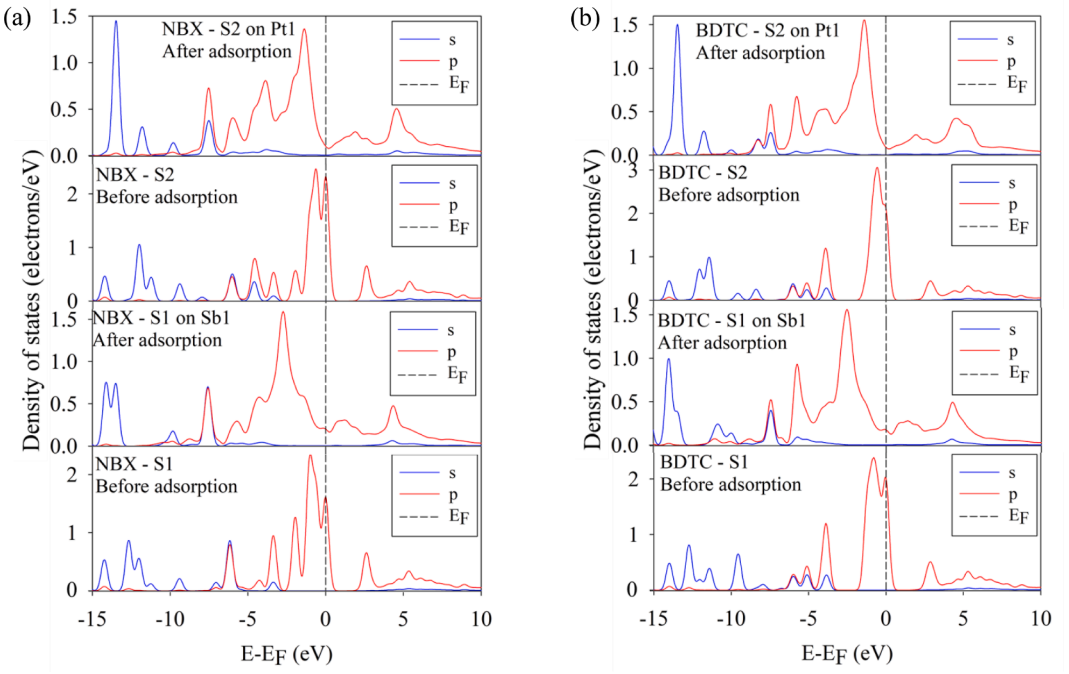

Fig. 12. The partial density of states (PDOS) of collector S atoms before and after adsorption on $PtSb_2$ (1 0 0) surface: (a) NBX^- and (b) $BDTC^-$.

collector S atoms lost charges, while Pt atoms gained charges. The charge gained on Pt atoms were 0.04|e⁻| after adsorption with NBX, BDTC and BTTC and 0.01|e⁻| after adsorption with DBDTP. This showed that Pt atoms gained more charges after interacting with NBX, BDTC and BTTC. Further examination of the magnitude of charges lost on the Sb atoms, revealed that 0.14|e⁻|, 0.15|e⁻|, 0.13|e⁻| and 0.20|e⁻| charges

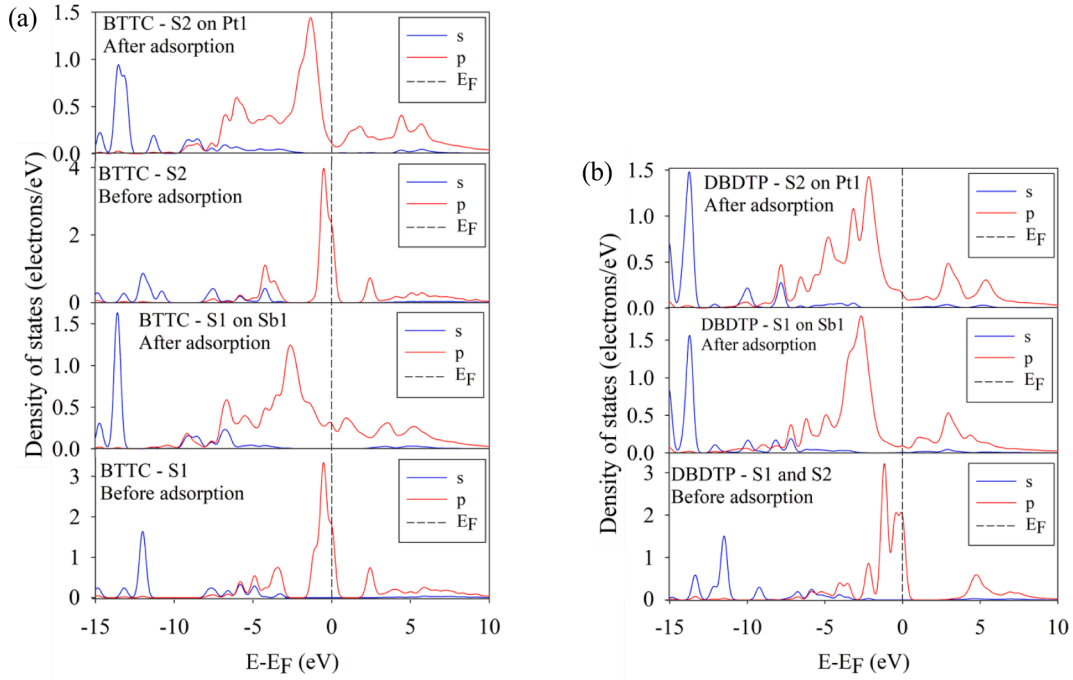

Fig. 13. The partial density of states (PDOS) of collector S atoms before and after adsorption on $PtSb_2$ (1 0 0) surface: (a) $BTTC^-$ and (b) $DBDTP^-$.

were lost after adsorption with NBX, BDTC, BTTC and DBDTP, respectively. This indicated that the Sb atoms lost more charges after interacting with DBDTP, and therefore the DBDTP was the greatest electron acceptor. This clearly showed that the Pt atoms were electron acceptors, while the Sb atoms were electron donors.

Table 8, also shows that there was a greater charge loss on the S2 atoms interacting with Pt1 atoms than on S1 atoms interacting with Sb1 atoms. This behaviour was due to Pt atom being an electron acceptor, while the Sb atom was an electron donor. The charges lost on the collectors S1 atoms were 0.31|e$^-$|, 0.34|e$^-$|, 0.29|e$^-$| and 0.33|e$^-$| for NBX, BDTC, BTTC and DBDTP, respectively. The charges lost on the S2 atoms were 0.35|e$^-$|, 0.40|e$^-$|, 0.32|e$^-$| and 0.41|e$^-$| for NBX, BDTC, BTTC and DBDTP, respectively. The computed charge sums (S1 + S2 charges) of the electrons lost on the S atoms were 0.66|e$^-$|, 0.74|e$^-$|, 0.61|e$^-$| and 0.74|e$^-$| for NBX, BDTC, BTTC and DBDTP, respectively. This clearly showed that BDTC and DBDTP lost more charges and the order of charge lost decreased as: BDTC = DBDTP > NBX > BTTC. These results indicated that the collectors S atoms offer their HOMO electrons to the Pt atoms LUMO orbitals, while the Sb atoms donate their 5p-orbital electrons to form a back donation covalent bond with the collectors S atoms. It was suggested that the charge loss on the S atoms occurred in order to form normal covalent stable bonds and some charges were localised on the bond.

4. Conclusions

This study compared the adsorption capacity of H_2O, OH^-, with NBX^-, $BDTC^-$, $BTTC^-$ and $DBDTP^-$ on platinum antimonide (geversite) (1 0 0) surface from bonding behaviour and adsorption energies using the density functional theory with dispersion correction method. The (1 0 0) surface was the most stable due to the lowest surface energy, which was also complemented by Wulff morphology for the $PtSb_2$ mineral. The partial density of states for the (1 0 0) surface indicated that the Sb atoms were more active than the Pt atoms. The full monolayer surface coverage adsorption of H_2O (−42.60 kJ.mol^{-1}) was found weaker than that of OH^- (−102.35 kJ.mol^{-1}), indicating that the OH^- had greater ability to bind on the geversite (1 0 0) surface. In addition the hydroxylation adsorbed through chemisorption, while hydration was though physisorption on the surface. The adsorption of collectors on the $PtSb_2$ (1 0 0) surface preferred bridging on the surface Pt and Sb atoms. The order of adsorption energies decreased as: BDTC (−406.38 kJ.mol^{-1}) > BTTC (−371.49 kJ.mol^{-1}) > NBX (−368.82 kJ.mol^{-1}) > DBDTP (−362.51 kJ.mol^{-1}), which showed that the BCTC exhibited the strongest exothermic adsorption. Significantly, it was found that the collectors bind stronger than water and OH^-, thus the collectors may easily displace water and OH^-, and attach on the mineral surface during flotation. The PDOS and atomic charges after adsorption showed that the Pt atoms gained charges, while the Sb atoms lost charges. Interestingly both collectors S atoms lost charges, with the S atoms interacting with Pt atoms losing greater charges. These results suggested that the collectors S atoms offered their HOMO electrons to the Pt atoms LUMO orbitals, while the Sb atoms donated their 5p-orbitals electrons to the collector S atoms to form normal covalent bonds and back donation covalent bonds on surface.

These results showed that the BDTC and BTTC are better collectors for flotation of geversite mineral. Moreover, the effect of N-bearing collector was found to improve the ability of the collector to bind onto geversite. Significantly, the study proposed that pH must be controlled to acidic or neutral in order to avoid strong effects of hydroxylation on the mineral surface, and therefore favour the interaction of collectors with mineral surface to render the platinum antimonide (geversite) mineral hydrophobic during the froth flotation process.

CRediT authorship contribution statement

Samuel S. Mangwejane: Formal analysis, Data curation, Writing - original draft. **Peace P. Mkhonto:** Formal analysis, Conceptualization, Supervision, Methodology, Writing - review & editing. **Phuti E. Ngoepe:** Formal analysis, Conceptualization, Supervision, Project administration, Funding acquisition.

Declaration of Competing Interest

The authors declare that they have no known competing financial interests or personal relationships that could have appeared to influence the work reported in this paper.

Table 8
Display the Mulliken atomic charges ($|e^-|$) of NBX^-, $BDTC^-$, $BTTC^-$ and $DBDTP^-$ collectors adsorptions on $PtSb_2$ (1 0 0) surface.

Collector	Atom	Adsorptions State	Atomic Population Charges				
			s	p	d	Total	Charge
NBX^-	Pt1	Before adsorption	0.98	0.94	9.06	10.98	−0.98
	Pt1	After adsorption	0.95	1.09	8.99	11.02	−1.02
	Sb1	Before adsorption	1.82	2.98	0.00	4.80	+0.20
	Sb1	After adsorption	1.81	2.85	0.00	4.66	+0.34
	S1	Before adsorption	1.83	4.53	0.00	6.36	−0.36
	S1	After adsorption	1.85	4.20	0.00	6.05	−0.05
	S2	Before adsorption	1.82	4.51	0.00	6.33	−0.33
	S2	After adsorption	1.82	4.16	0.00	5.98	+0.02
$BDTC^-$	Pt1	Before adsorption	0.98	0.94	9.06	10.98	−0.98
	Pt1	After adsorption	0.95	1.09	8.98	11.02	−1.02
	Sb1	Before adsorption	1.82	2.98	0.00	4.80	+0.20
	Sb1	After adsorption	1.80	2.84	0.00	4.65	+0.35
	S1	Before adsorption	1.83	4.57	0.00	6.41	−0.41
	S1	After adsorption	1.85	4.22	0.00	6.07	−0.07
	S2	Before adsorption	1.84	4.60	0.00	6.43	−0.43
	S2	After adsorption	1.82	4.20	0.00	6.03	−0.03
$BTTC^-$	Pt1	Before adsorption	0.98	0.94	9.06	10.98	−0.98
	Pt1	After adsorption	0.95	1.08	8.99	11.02	−1.02
	Sb1	Before adsorption	1.82	2.98	0.00	4.80	+0.20
	Sb1	After adsorption	1.81	2.86	0.00	4.67	+0.33
	S1	Before adsorption	1.83	4.47	0.00	6.30	−0.30
	S1	After adsorption	1.85	4.17	0.00	6.01	–0.01
	S2	Before adsorption	1.83	4.47	0.00	6.30	−0.30
	S2	After adsorption	1.82	4.15	0.00	5.98	+0.02
$DBDTP^-$	Pt1	Before adsorption	0.98	0.94	9.06	10.98	−0.98
	Pt1	After adsorption	0.92	1.06	9.01	10.99	−0.99
	Sb1	Before adsorption	1.82	2.98	0.00	4.80	+0.20
	Sb1	After adsorption	1.78	2.83	0.00	4.60	+0.40
	S1	Before adsorption	1.88	4.87	0.00	6.75	−0.75
	S1	After adsorption	1.89	4.52	0.00	6.42	−0.42
	S2	Before adsorption	1.88	4.87	0.00	6.75	−0.75
	S2	After adsorption	1.86	4.48	0.00	6.34	−0.34

Data availability

No data was used for the research described in the article.

Acknowledgement

This work performed at the Materials Modelling Centre in University of Limpopo. Financial support was received from the Department of Science and Innovation (DSI) and National Research Foundation (NRF) South African Research Chair Initiative (SARChI) (Grant ID: 61414). The computational work benefited from supercomputing resources at the Centre for High Performance Computing (CHPC).

Appendix A. Supplementary material

Supplementary data to this article can be found online at https://doi.org/10.1016/j.commatsci.2023.112174.

References

[1] C.T. O'Connor, N.J. Shackleton, Investigations into the recovery of platinum group minerals from the platreef ore of the Bushveld Complex of South Africa, Platinum Met. Rev. 57 (4) (2013) 302–309.
[2] R. Sefako, V. Sibanda, K. Sekgarametso, PGM extraction from oxidized ores using flotation and leaching, J. S. Afr. Inst. Min. Metall. 119 (2019) 929–936.
[3] E.F. Stumpfl, Some new platinoid-rich minerals, identified with the electron microanalyser, J. Mineral. Soc. 32 (1961) 833–847.
[4] C.N. Waterson, P.A. Tasker, R. Farinato, D.R. Nagaraj, N. Shackleton, A computational and experimental study on the binding of dithio ligands to sperrylite, pentlandite and platinum, J. Phys. Chem. C 120 (2016) 22476–22488.
[5] M. Tarkian, E.F. Stumpf, Platinum mineralogy of the Driekop mine, South Africa, Miner. Deposita 10 (1975) 71–85.
[6] P.R. Emtage, Band structure of platinum antimonide, Phys. Rev. 138 (1965) A246–A259.
[7] D.H. Damon, R.C. Miller, A. Sagar, Semiconducting properties of PtSb2, Phys. Rev. 138 (1965) A636–A645.
[8] P.E. Ngoepe, P.S. Ntoahae, S.S. Mangwejane, H.M. Sithole, S.C. Parker, K.V. Wright N.H d. Leeuw, Atomistic simulation studies of iron sulphide, platinum antimonide and platinum arsenide, S, Afr. J. Sci. 101 (2005) 480–483.
[9] S.S. Mangoejane, Density Functional Theory Studies of O_2, H_2O, OH^- and Xanthates Adsorption on Platinum Antimony ($PtSb_2$) Surfaces. Polokwane, Limpopo, South Africa: PhD Thesis, University of Limpopo (2020).
[10] P.P. Mkhonto, X. Zhang, L. Lu, W. Xiong, Y. Zhu, L. Han, P.E. Ngoepe, Design, synthesis and investigating the interaction of novel s-triazine collector with pyrite surface: A DFT-D3+U and experimental studies, Surf. Interfaces 38 (102820) (2023) 1–16.
[11] V.A. Chanturia, T.V. Nedosekina, V.V. Stepanova, Experimental-analytical methods of the investigating the effects of complex reagesnts on platinum flotation, J. Min. Sci. 44 (3) (2008) 283–288.
[12] C.F. Vos, J.C. Davidtz, J.D. Miller, Trithiocarbonates for PGM flotation, J. S. Afr. Inst. Min. Metall. 107 (2007) 1–6.
[13] B. Nemutudi, P.P. Mkhonto, P.E. Ngoepe, Oxidation behaviour of sperrylite and platarsite (100) surfaces: A DFT study, Mater. Today Commun. 32 (103868) (2022) 1–11.
[14] P.S. Ntoahae, Application of computer simulation methods to the study of platinum group minerals, Ph.D. thesis. Polokwane, Limpopo, South Africa: University of Limpopo, Turfloop (2005).
[15] S.T. Ntobeng, P.P. Mkhonto, M.A. Mehlape, P.E. Ngoepe, Computational Modelling Studies of Pentlandite $(Fe,Ni)_9S_8$ (111) surface: Oxidation and hydration, SAIP2021 Proceedings (2021) 43-48.
[16] A. Tkatchenko, M. Scheffler, Accurate molecular Van der Waals interactions from ground-state electron density and free-atom reference data, Phys. Rev. Lett. 102 (2009) 1–4.
[17] J.P. Perdew, K. Burke, M. Ernzerhof, Generalized gradient approximation made simple, Phys. Rev. Lett. 77 (1996) 3865–3868.
[18] S.J. Clark, M.D. Segall, C.J. Pickard, P.J. Hasnip, M.J. Probert, K. Refson, M. C. Payne, First principle methods using CASTEP, Z, Kristalography-Crystalographic Materials (2005) 567–570.
[19] H.F. Monkhorst, J.D. Pack, Special points for Brillouin-zone integrations, Phys. Rev. B 13 (1976) 5188–5192.
[20] H. Yan, M. Zhang, Theoretical investigation on compressibility, electronic and thermodynamic properties of single crystal $PtAs_2$ under high pressure, Comput. Mater. Sci. 86 (2014) 124–129.
[21] G. Makov, M.C. Payne, Periodic boundary conditions in ab Initio calculations, Phys. Rev. B: Condens. Matter Mater. Phys. 51 (1995) 4014–4022.
[22] H.P. Komsa, T.T. Rantala, A. Pasquarello, Finite-size supercell correction schemes for charged defect calculations, Phys. Rev. B 86 (2012) 1–16.
[23] N.Y. Dzade, N.H. de Leeuw, Adsorption and desulfurization mechanism of thiophene on layered FeS(001), (011), and (111) surfaces: A dispersion-corrected density functional theory study, J. Phys. Chem. C 122 (2018) 359–370.

[24] B. McFadzean, P. Mkhonto, P.E. Ngoepe, Interactions of xanthates of increasing chain length with pyrite surfaces: A DFT-D and microcalorimetry study, Appl. Surf. Sci. 607 (154910) (2023) 1–13.
[25] J. Neugebauer, M. Scheffler, Adsorbate-substrate and adsorbate-adsorbate interactions of Na and K adlayers on Al(111), Phys. Rev. B: Condens. Matter Mater. Phys. 46 (1992) 16067–16080.
[26] W. Sun, G. Ceder, Efficient creation and convergence of surface slabs, Surf. Sci. 617 (2013) 53–59.
[27] X. Tian, T. Wang, L. Fan, Y. Wang, H. Lu, Y. Mu, A DFT based method for calculating the surface energies of asymmetric MoP facets, Appl. Surf. Sci. 427 (2018) 357–362.
[28] B. Nemutudi, P.P. Mkhonto, P.E. Ngoepe, Ab initio studies of sperrylite, platarsite and palladoarsenide bulk and surface stabilities, SAIP2019 Proceedings (2019) 6-11.
[29] P.P. Mkhonto, X. Zhang, L. Lu, W. Xiong, Y. Zhu, L. Han, P.E. Ngoepe, Adsorption mechanisms and effects of thiocarbamate collectors in the separation of chalcopyrite from pyrite minerals: DFT and experimental studies, Miner. Eng. 176 (107318) (2022) 1–14.
[30] A. Hung, J. Muscat, I. Yorovsky, S.P. Russo, Density functional theory studies pyrite FeS_2 (100) and (110) surfaces, Surf. Sci. 513 (2002) 511–524.
[31] P.W. Tasker, Stability of ionic crystal surfaces, J. Phys. C: Solid State Phys. 12 (1979) 4977–4984.
[32] T.G. Cooper, N.H. de Leeuw, A computer modelling study of the incorporation of K^+, Ca^{2+} and Mg^{2+} impurities in two Na_2SO_4 polymorphs: Introducing a Na_2SO_4 potential model, J. Cryst. Growth 294 (2006) 137–149.
[33] N.H. de Leeuw, T.C. Cooper, Surface simulation studies of the hydration of white rust $Fe(OH)_2$, goethite a-FeO(OH) and hematite a-Fe_2O_3, Geochim. Cosmochim. Acta 71 (2007) 1655–1673.
[34] G. Wulff, Zur Frage der Geschwindigkeit des Wachstums und der Auflösung der Krystallflagen, Z. Kristallogr. Miner. 34 (1901) 449–530.
[35] J.W. Gibbs, The collected works of J. Willard Gibbs, New York: Longmans, Green (1928) 1839-1903.
[36] P.P. Mkhonto, P.E. Ngoepe, Reconstruction of cooperite (PtS) surfaces: A DFT-D+U study, ACS Omega 7 (48) (2022) 43390–43410.
[37] V.I. Rozhdestvina, A.A. Udovenko, S.V. Rubanov, N.V. Mudrovskaya, Structural investigation of cooperite (PtS) crystals, crystallogr, Rep. 61 (2016) 193–202.
[38] C.N. Waterson, Design, synthesis and testing of reagents for high-value mineral collection, Edinburgh, United Kingdom, Scotland: PhD Thesis, The University of Edinburgh (2015).
[39] J. Chen, X. Long, Y. Chen, Comparison of multilayer water adsorption on the hydrophobic galena (PbS) and hydrophilic pyrite (FeS2) surfaces: A DFT study, J. Phys. Chem. C 118 (2014) 11657–11665.
[40] T.A. Albright, J.K. Burdett, M.-H. Whangbo, Orbital interactions in chemistry, J. Wiley u. Sons, New York, Chichester, 1985.
[41] P.P. Mkhonto, X. Zhang, L. Lu, Y. Zhu, L. Han, P.E. Ngoepe, Unravelling the performance of oxycarbonyl-thiocarbamate collectors on chalcopyrite using first-principles calculations and micro-flotation recoveries, Appl. Surf. Sci. 563 (150332) (2021) 1–13.
[42] B. McFadzean, C.T. O'Connor, A thermochemical study of thiol collector surface reactions on galena, Miner. Eng. 65 (2014) 54–60.
[43] P.P. Mkhonto, H.R Chauke, P.E. Ngoepe, The effect of thiol collectors on nickel-rich (110) pentlandite surface using density functional theory, Proceedings of SAIP2017 (2018) 95–100.